

Momentum-Resolved Dielectric Response of Free-Standing Mono-, Bi-, and Trilayer Black Phosphorus

Etienne Gaufrès,^{*,†,✉,○} Frédéric Fossard,[†] Vincent Gosselin,[‡] Lorenzo Sponza,[†] François Ducastelle,[†] Zhenglu Li,^{§,✉,#} Steven G. Louie,^{§,✉,#} Richard Martel,^{||} Michel Côté,[‡] and Annick Loiseau^{*,†}

[†]Laboratoire d'Etude des Microstructures, ONERA-CNRS, UMR104, Université Paris-Saclay, BP 72, 92322 Châtillon Cedex, France

[‡]Département de Physique, Université de Montréal, Montréal QC H3C 3J7, Canada

[§]Department of Physics, University of California at Berkeley, Berkeley, California 94720, United States

^{||}Département de Chimie, Université de Montréal, Montréal QC H3C 3J7, Canada

[○]LP2N, Laboratoire Photonique Numérique et Nanosciences, Univ. Bordeaux, F-33400 Talence, France

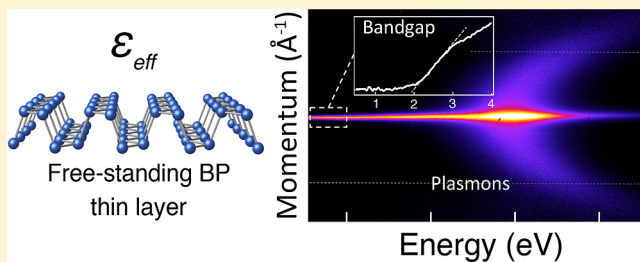
[✉]Institut d'Optique & CNRS, UMR 5298, F-33400 Talence, France

[#]Materials Sciences Division, Lawrence Berkeley National Laboratory, Berkeley, California 94720, United States

S Supporting Information

ABSTRACT: Black phosphorus (BP), a 2D semiconducting material of interest in electronics and photonics, exhibits physical properties characterized by strong anisotropy and band gap energy that scales with reducing layer number. However, the investigation of its intrinsic properties is challenging because thin-layer BP is photo-oxidized under ambient conditions and the energy of its electronic states shifts in different dielectric environments. We prepared free-standing samples of few-layer BP under glovebox conditions and probed the dielectric response in a vacuum using scanning transmission electron microscopy and electron energy loss spectroscopy (STEM-EELS). Thresholds of the excitation energy are measured at 1.9, 1.4, and 1.1 eV for the mono-, bi-, and trilayer BP, respectively, and these values are used to estimate the corresponding optical band gaps. A comparison of our results with electronic structure calculations indicates that the variation of the quasi-particle gap is larger than that of the exciton binding energy. The dispersion of the plasmons versus momentum for one- to three-layer BP and bulk BP highlights a deviation from parabolic to linear dispersion and strong anisotropic fingerprints.

KEYWORDS: 2D semiconductor, black phosphorus, bandgap, dielectric properties, plasmons, EELS



Black phosphorus (BP) stands out from other 2D materials in the photonic and optoelectronic fields due to the high carrier mobility, about a few thousands of $\text{cm}^2 \text{ V}^{-1} \text{ s}^{-1}$ for holes, and a band gap that depends on layer thickness.^{1–5} Composed of tetravalent phosphorus atoms in a quasi sp^3 hybridization, the puckered and lamellar structure of BP enables mechanical exfoliation of few-layer BP, giving a modulation of the optical band gap from ~ 0.35 eV in the bulk BP to roughly 2 eV for the monolayer.^{2,6,7} Additionally, the band gap remains direct for any layer number.^{3,7,8} This unusual behavior in the panorama of 2D semiconductors is of high interest in various fields of photonics, such as light harvesting, climate monitoring (0.5 eV), telecommunication wavelengths (0.8 eV), and silicon photonics (1.1 eV).⁹

Confinement effects in semiconducting nanomaterials induce, however, a significant renormalization of energy terms, which reshapes the dielectric response across the whole spectrum (0–30 eV) where interband transitions and plasmon resonances are found. In the case of ultrathin layers, the nonlocality of the dielectric function can further tune the

optical properties of nanomaterials and exacerbates the material's sensitivity to environmental effects and dielectric surroundings.^{10,11} Such effects are dominant, for example, in carbon nanotubes (1D) and exfoliated transition metal dichalcogenides (TMDCs) (2D).^{12–16} For few-layer BP, it is therefore expected that both quantum confinement and interface effects influence the optical response.^{17,18} Hence, mapping the intrinsic dielectric response of ultrathin BP layers under reference conditions will provide the foundation for a key data set of the optical response of BP and help in predicting band gap energy with layer number in a complex dielectric environment, such as in BP-based van der Waals (VdW) heterostructures.

Here, we measure the energy electron loss spectra (EELS) in the 1–30 eV range of mono-, bi-, and trilayer and bulk BP suspended in a vacuum in a high-resolution transmission electron microscope (HRTEM) operated at 80 and 40 kV. A

Received: September 23, 2019

Published: October 11, 2019

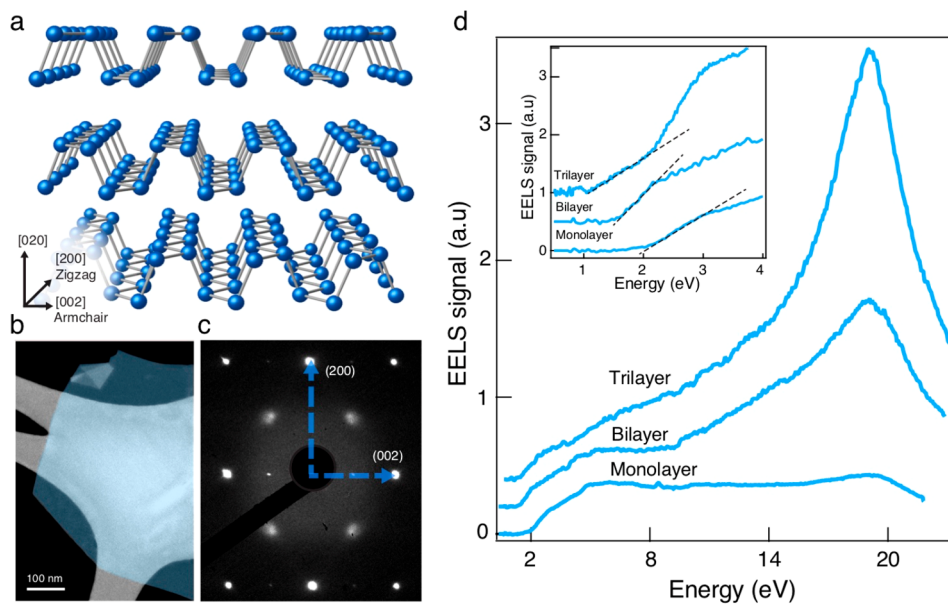


Figure 1. Crystallographic structure and EELS response of exfoliated BP suspended in a vacuum. (a) Schematic description of the BP atomic structure and its crystallographic axis. (b) HAADF contrast image recorded at 80 kV of a bilayer BP exfoliated on a TEM grid. The layer is colored in blue for clarity. (c) Assignment of the armchair and zigzag orientations [002] and [200], respectively, in the diffraction pattern recorded from an exfoliated few-layer BP. (d) Electron energy loss spectroscopy (EELS) spectra at 80 kV in the range (1–23 eV) of the mono-, bi-, and trilayer BP. Inset: High-resolution valence-EELS (1–5 eV) spectra displaying thresholds at 1.9, 1.4, and 1.1 eV for the mono-, bi-, and trilayer BP, respectively.

significant shift of the band gap threshold of free-standing samples is obtained compared to the reported values in other dielectric environments, such as SiO_2 and hexagonal boron nitride (h-BN). Using *ab initio* Bethe–Salpeter simulations coupled to a variational model, we ascribe this shift to a strong layer dependent modulation of both the exciton binding energy, E_b , and the band gap energy with the dielectric environment. For the BP monolayer, the amplitude of the modulation reaches up to 0.6 eV when the average environmental dielectric function varies from 1 to 40. Furthermore, the EELS responses of the surface and volume plasmons for one- to three-layer and bulk BP as a function of momentum show strong anisotropic confinement effects in the armchair and zigzag directions and specific fingerprints that are consistent with our *ab initio* results.

Experiments. The dielectric response of few-layer BP is probed using EELS signals acquired with a transmission electron microscope (Zeiss Libra 200 MC) equipped with an electrostatic CEO5 monochromator, an in-column filter, and a Gatan ultrascan 1000 CCD camera. The microscope operates at 40 or 80 kV to avoid knock-on damage and exhibits an energy resolution of 100 meV. To avoid layer degradation, black phosphorus samples are exfoliated in a glovebox with oxygen and moisture levels below 1 ppm using a PDMS stamp.⁶ The thin layers are then transferred from the stamp to a holey carbon TEM grid using direct contact (*Supporting Information*). The TEM grid is placed on the sample holder inside the glovebox and then transferred into the microscope under an inert atmosphere. The layer number is estimated using HRTEM phase contrast images and high annular angle dark field (TEM-HAADF) Z-contrast images following a procedure described in our previous work (*Supporting Information*).⁶ During analysis, the flake is oriented to obtain the main crystallographic directions armchair [002] and zigzag [200] in the diffraction pattern ([010] zone axis) (Figure 1a and c). In this configuration, an area of about 100 nm in

diameter, free of eventual impurity and at a minimum distance of 30 nm from another flake or thickness change, is selected to perform the EELS experiments (see the Supporting Information, Figure S0).

Optical and Electronic Band Gaps. We first studied the impact of 2D quantum confinement on the valence band edge excitations of ultrathin BP layers suspended in a vacuum. For that purpose, we selected free-standing layers displaying HAADF contrasts consistent of exfoliated BP samples having one, two, and three layers; as an example, the bilayer is illustrated in Figure 1b. Note that measurements have been repeated on other samples with the same results (Figures S1–S9, Supporting Information). The EELS spectra in the range between 0 and 4 eV of the corresponding layers (inset of Figure 1d) are used to evaluate excitation threshold energies of 1.9 ± 0.1 , 1.4 ± 0.1 , and 1.1 ± 0.1 eV for one-, two-, and three-layer BP, respectively, using the tangential method, which is a standard analysis method applied to semiconductors.^{19–25} As shown in the Supporting Information, this empirical method leads to reproducible values of the threshold (see in particular Figure S6). A comparison of these values with optical band gap energies, E_α , of few-layer BP reported in the literature (Table S1, Supporting Information) indicates a slightly blue-shifted resonance of about 0.25 eV on average (Table S3, Supporting Information). At first sight, this discrepancy can be ascribed to the fundamental difference between EELS and optical spectroscopies. As further detailed in the Supporting Information, we show, however, that the difference between band gap energy values obtained with EELS and optical absorption is negligible (within 0.1 eV at most) in the case of BP and that the blue shift measured here is mainly due to a difference in environmental screening. In short, the experimental optical absorption and EELS loss function are indeed intrinsically different, with the former being proportional to $\text{Im}[\epsilon(\omega)]$ and the latter to $-\text{Im}[1/\epsilon(\omega)]$, but the magnitude of this difference depends on the strength of the excitonic

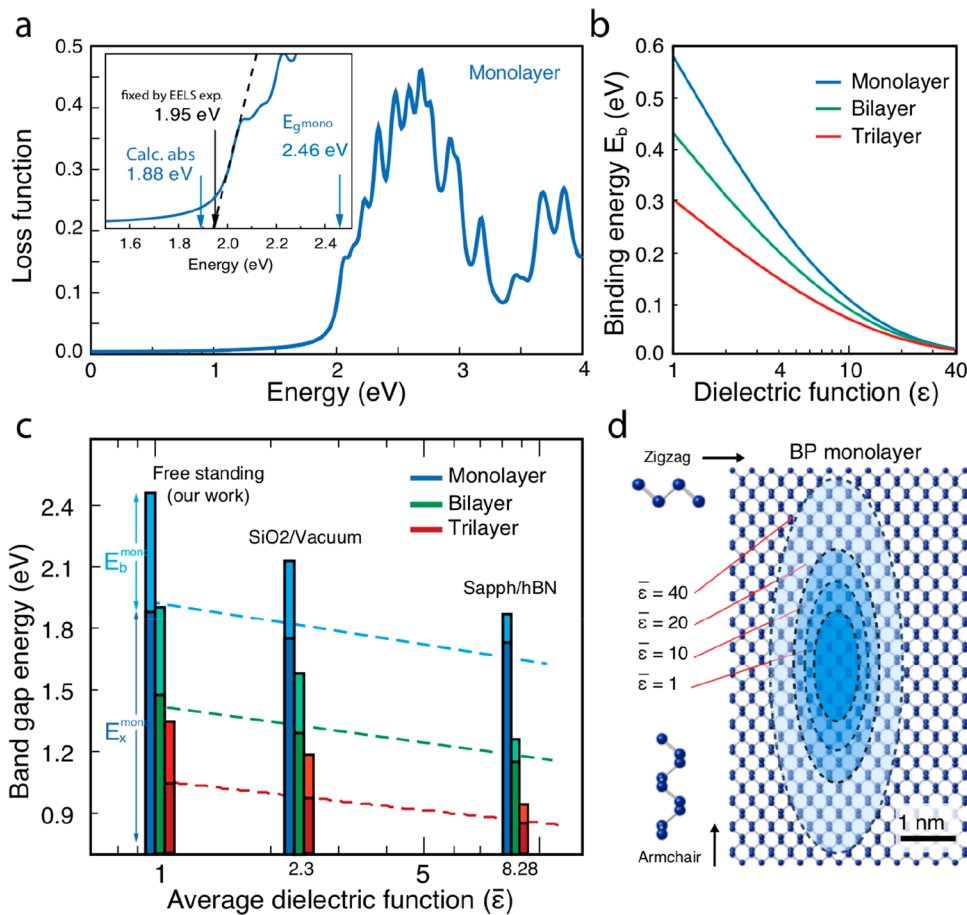


Figure 2. Dielectric screening effects on band gap and exciton binding energy in few-layer BP. (a) BSE loss function of the monolayer. Inset: Close-up on the spectral onset. Arrows mark the energy gaps obtained by the same extrapolation method employed using the experimental EELS results (black arrow) and the calculated absorption peak (blue arrows). (b) Exciton binding energies as a function of the average environmental dielectric function $\bar{\epsilon}$. (c) Optical gaps E_x (dark segments) and exciton binding energies E_b (light segments) in different dielectric environments. The optical gaps are experimental data coming from the literature (see Table S3) and from this work. The dashed lines are linear interpolations of the experimental data to guide the eyes. (d) Representation of the simulated excitonic radii for the monolayer in the armchair and zigzag directions for different dielectric environments.

effects: When the excitonic peak is strong and far from the continuum of interband transitions, such as in h-BN, the threshold of the two spectra may differ substantially. However, Kramers–Kronig relations imply similar structures between EELS and absorption spectra when excitonic effects are weak. For BP layers, we evaluated this difference using values obtained by EELS as a reference input for calculations. To do so, we compared simulated spectra of $\text{Im}[\epsilon(\omega)]$ and $-\text{Im}[1/\epsilon(\omega)]$ in the mono-, bi-, and trilayer BP by solving the Bethe–Salpeter equation (BSE), while quasiparticle effects have been included by shifting the Kohn–Sham empty states by an amount which ensures that the experimental thresholds match those extracted from the simulated loss function using the same tangential method. All parameters of the calculations can be found in the Supporting Information. As an example, this analysis carried out on the monolayer is shown in the inset of Figure 2a, where blue arrows indicate the quasiparticle gap ($E_g = 2.46$ eV), and the optical gap derived from absorption spectra (peak of $\text{Im}[\epsilon(\omega)]$). Note that the electronic band gap value obtained for the monolayer in a vacuum is in very good agreement with the value recently predicted by Frank et al. by using many-body quantum Monte Carlo calculations.²⁶ In all three cases, the corresponding optical gap extracted from the loss function is less than 0.1 eV higher than the EELS

threshold, which is within the experimental error bar. Therefore, we conclude that the measured EELS threshold values are representative of the optical gap energies of the free-standing BP layers considered here.

Ruling out the mismatch between EELS and optical absorption measurements and assuming that the dielectric screening of the surrounding can significantly impact the electronic band gap and the binding energy, E_b , of the excitons, it appears that the 0.25 eV blue shift of the threshold energies is due to the different dielectric environments between our free-standing samples and other samples in the literature, which are all supported on a substrate. To test this hypothesis, we developed a variational model based on a generalization of the approach introduced by Prada et al.²⁷ that describes the excitons in a planar geometry. In our model, the system is composed of a thin slab of BP sandwiched between two semi-infinite dielectrics ϵ_1 and ϵ_2 , which contribute to the screening through an average dielectric function $\bar{\epsilon}$ (see the Supporting Information). We first computed $E_b(\bar{\epsilon})$, and the calculations indicate a strong dependency of E_b on $\bar{\epsilon}$ with a maximum amplitude variation of about 0.6 and 0.3 eV in the range $1 < \bar{\epsilon} < 40$ for the monolayer and trilayer BP, respectively (Figure 2b). Hence, the thinner the BP film, the stronger is the effect of screening by the environment on the optical properties.

Furthermore, the impact of quantum confinement with reducing layer number on the excitonic properties vanishes when the dielectric environment provides strong screening. Consistently, the in-plane excitonic radii, a_x and a_y extracted from the model, increase for increasing $\bar{\epsilon}$ due to reduced electron–hole attraction and their values are significantly different owing to the anisotropy of the system (Figure 2d). These radii quantify the extension of the electron–hole pair in the two orthogonal directions and highlight the strong anisotropy of BP where the exciton is elongated along the armchair direction. In the model, this anisotropy is taken into account by the effective mass of the electron–hole pair μ_{eh} , which is larger for the zigzag direction (x) than for the armchair direction (y). Note also that the model predicts an anisotropy factor $\lambda = a_y/a_x$ almost constant in all environments for the three systems (around 2.5 in the monolayer and the bilayer and around 2.3 in the trilayer).

As shown in Figure 2c and based on our experimental data set and the optical gap values, $E_x(\bar{\epsilon})$, found in the literature^{7,28} (see also Table S3), a simulated abacus can be drawn to provide an estimate of the quasiparticle gap ($E_g = E_x + E_b$) expressed as the sum of the optical gap (E_x) and the corresponding exciton binding energy (E_b) for various effective dielectric constants simulating various experimental conditions. This abacus enables one to rationalize the already diverse experimental data published on few-layer BP and show the strong impact of the surroundings on the optoelectronic properties of thin-layer BP, which is relevant in the context of BP passivation or after integration in heterostructures.²⁹

A usual assumption in the context of nano-objects is that the environmental dielectric screening significantly shifts the binding energy of the exciton and renormalizes the fundamental gap and that these changes of opposite sign compensate almost exactly, resulting in a weak dependence of E_x on the (environmental) screening. This hypothesis has been put forward in theoretical works on carbon and h-BN nanotubes³⁰ and recently reaffirmed by Qiu et al. on free-standing and supported few-layer BP.¹⁸ What emerges from our study is that E_x decreases nevertheless with larger screening. Giving that dielectric effects in exfoliated BP drive changes of E_b and E_g , the reduction of E_g appears sizably larger than the reduction of E_b .

Dispersions of Plasmons. In another set of experiments, we probed the dielectric response of ultrathin BP samples in the range 10–40 eV and its dispersion as a function of the momentum q . The details of our TEM apparatus for dispersive EELS recording can be found in the Supporting Information and in the work by Fossard et al.³¹ In Figure 3a, we compared the dispersion of the dielectric response in the bilayer BP for two values of momentum close to 0, i.e., $q = 0 \text{ \AA}^{-1}$ and $q = 0.2 \text{ \AA}^{-1}$. It appears clearly that the near band edge part of the dielectric response rapidly vanishes and cannot be resolved with our setup. This is consistent with the selection rules related to optical processes for nonzero values of the momentum and with the exciton dispersion predicted for BP and other 2D materials.^{32,33}

Now, we focus on the dispersion of the plasmonic contributions, which is characterized by a maximum intensity at 19.3 eV (for $q = 0 \text{ \AA}^{-1}$), using the TEM in-column energy filter to record the scattering pattern at fixed energies (EFSP). Figure 3b shows the intensity repartition of the dielectric function as a function of momentum and direction for fixed values of energy. At 19 eV, the intensity maximum of the

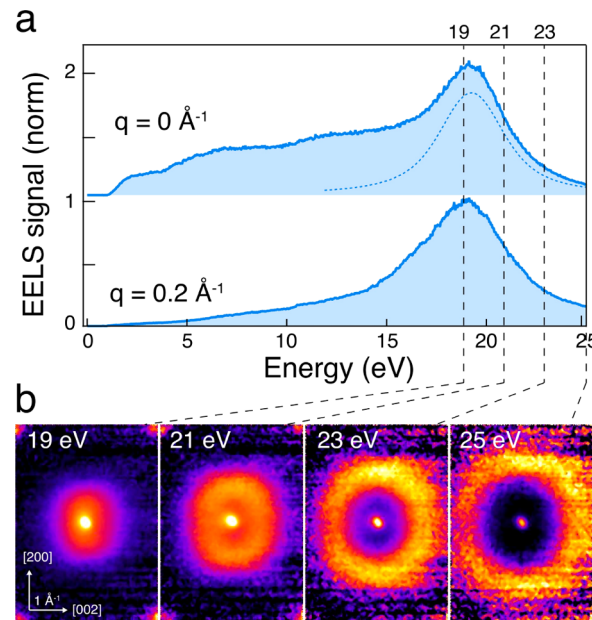


Figure 3. Energy filtered TEM-EELS. (a) Momentum-resolved EELS spectra at $q = 0 \text{ \AA}^{-1}$ and $q = 0.2 \text{ \AA}^{-1}$ from a bilayer BP. (b) Energy filtered scattering patterns (EFSPs) measured at different energies in the plasmon dispersion range. Experiments were done with an accelerating voltage of 80 kV.

plasmon is consistently concentrated on values of q close to 0 \AA^{-1} .^{34,35} The extraction of the scattering pattern performed at higher energies, i.e., $E = 21, 23$, and 25 eV , reveals a significant dispersion of the maximum intensity with an elongated donut shape in the zigzag direction (i.e., [200]). This feature highlights the impact of the structural anisotropy of BP on the plasmon dispersion.

To better scrutinize this anisotropic fingerprint in the plasmonic dispersion, we created ω - q maps according to a TEM configuration reported in ref 31 with an energy and momentum resolution of 0.1 eV and 0.1 \AA^{-1} , respectively. As an example, the ω - q map of bulk BP losses along the armchair direction is plotted in Figure 4a. The intensity of the raw EELS signal is corrected by a q^2 factor, which comes from the nature of the recorded signal $S(q) = -(1/q^2) \text{Im}(1/\epsilon)$. For clarity, an offset is also applied so that the figure does not display a black line at $q = 0$. The two branches of the plasmon dispersion are clearly identified, even beyond the Brillouin zone limit, and characterized by an amplitude shift of more than 5 eV. Thanks to the in-plane rotation of the specimen holder, we repeated the experiment after rotating the same flake in the TEM chamber by an in-plane angle of 90° to record the contributions in the zigzag direction. From the EFSP or ω - q experiments, the plasmon spectra were extracted from the datacube, as demonstrated in Figure 4b, for a trilayer BP.

In Figure 4c, the plasmon dispersions for the mono-, bi-, and trilayer BP and bulk BP are compared together. Each dotted point corresponds to the position of the plasmon energies along the armchair and zigzag directions. In a complementary way, we also calculated the EELS response of bulk and monolayer BP by directly computing the dielectric function using a first-principles approach in the following way: First, the ground state electronic structure is obtained with the ABINIT code,³⁶ and then, the electronic states are processed by the BerkeleyGW code³⁷ in order to compute the dielectric

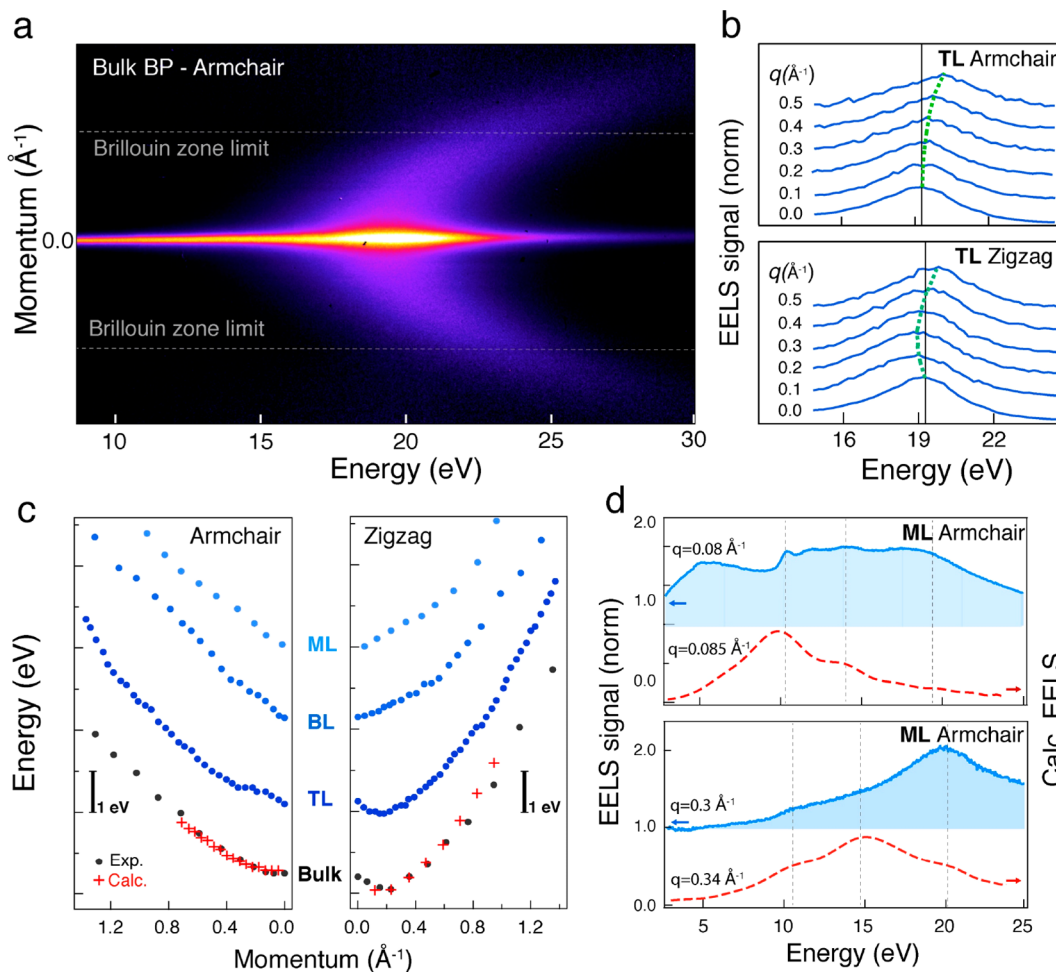


Figure 4. Plasmon dispersion in the armchair and zigzag directions in few-layer BP. (a) ω - q map of the plasmon losses centered at 19.3 eV along the armchair direction. (b) Momentum-resolved plasmon losses extracted from ω - q experiments of a trilayer BP along the armchair (top) and zigzag (bottom) directions. (c) Maximum volume plasmon peak energy as a function of momentum and crystallographic orientations (armchair and zigzag). The data are extracted from the ω - q maps recorded from exfoliated mono-, bi-, and trilayer (ML, BL, TL) BP and bulk BP. The simulated data for the bulk are indicated by red crosses. The ML, BL, TL, and bulk dispersions are up-shifted for clarity. (d) Measured (continuous blue) and calculated (dashed red) EELS signals of monolayer BP for $q \sim 0 \text{ \AA}^{-1}$ and $q \sim 0.3 \text{ \AA}^{-1}$.

response of the system within the random phase approximation. We then extract the momentum and frequency dependence of the dielectric function. The red crosses correspond to the plasmon energies calculated in the bulk and show good agreement with experimental data. The features of the plasmon dispersions presented in Figure 4c are therefore identified as being intrinsic of bulk BP material.

These results of the dispersion present clear deviations from the well-known parabolic \sqrt{q} dependency of a plasmon dispersion in 2D systems, with specific fingerprints compared to bulk for the armchair and zigzag directions for monolayer and bilayer BP. First, the dispersion amplitude is asymmetrically higher for the zigzag direction than for the armchair direction. As already put forward for accounting for the anisotropic extension of excitons in Figure 2c, this anisotropy of the EELS response corroborates the theoretical prediction by Gosh et al. obtained using the TDDFT framework³⁸ that it is most likely linked to the difference of effective mass between the main orthogonal directions.³⁹ Second, another non-parabolic behavior and asymmetric inversion centers of the dispersion in the range from 0 to 0.3 \AA^{-1} are identified for the zigzag direction, as highlighted in Figure 4b. Still present for

trilayer BP, the origin of this unexpected deviation is unclear but could be induced by an effective interband coupling promoted because of the small values of the bulk-like band gap energies.³⁹ This hypothesis is supported by the fact that this deviation is quite attenuated in the bilayer and monolayer for which the band gap energies (1.45 and 1.9 eV, respectively) are much larger compared to bulk BP (0.35 eV) and even so for the trilayer (1.1 eV). Therefore, the attenuation of the nonparabolic behavior in mono- and bilayer samples appears to be a fingerprint of the important change in band gap. It also means that plasmonic properties of BP films behave as bulk above three layers.

The electronic dispersion of the bilayer also stands out from that of the trilayer and bulk by the apparent loss of the parabolic dispersion toward a linearization of the plasmon dispersion. This quantum confinement effect was already observed in low-dimensional materials such as carbon nanotubes and graphene by Kramberger et al.⁴⁰ For high momentum values, i.e., interaction distances of a few Angstroms representing small fractions of the film thickness, the suppression of the neighboring effect in bilayer and monolayer may induce this linearization of the dispersion of plasmons.

Last, the plasmon response of a monolayer BP suspended in a vacuum shown in Figure 4d is now discussed in more detail using support from calculated spectra. The EELS spectra for near-zero values of momentum in the armchair direction show a strong decrease of the contribution from the volume plasmon at 19.3 eV compared to the near-band-edge contribution (1–5 eV). This is consistent with a volume plasmon vanishing when the thickness approaches values close to zero. Another feature in Figure 4d is the very broad heterogeneous signal starting from 10 to 20 eV with structuration at 10 and 14 eV. This signal is also noticeable, although weaker, in the bilayer EELS spectra presented in Figure 3a. The contribution at 10 eV has been observed in thin BP layers by Wu et al. and ascribed to high energy surface plasmons.³⁴ In comparison, the calculated EELS spectrum shows clear plasmonic contributions at 10 and 13.5 eV, which are coupled to a weak and broad contribution at around 20 eV. Besides the relative intensity, the positions of these features are in agreement with our experimental data. When comparing the experimental and simulated EELS responses of the monolayer for a momentum value of 0.3 Å⁻¹ (Figure 4d, bottom), it appears that the relative intensities of the contributions are modulated and that the decrease of the near-band-edge signal is effective with the main contribution at 20 eV and two minor contributions at 11 and 15 eV, shifted by about 1 eV compared to the spectra at $q \sim 0$ Å⁻¹. This shift is similar to those observed for the mono-, bi-, and trilayer BP and bulk BP dispersions with an average dispersion rate of 4 eV per Å⁻¹ with also a clear linearization effect between 0 and 1 Å⁻¹, comparable to what was already noticed for the bilayer (Figure 4c). The simulation also shows a similar shift of the surface and volume plasmon contributions in the EELS spectra calculated at 0.34 Å⁻¹ but with a less intense modulation of the relative intensity between surface and volume contributions.

In conclusion, we have measured the dielectric response of free-standing BP layers using EELS spectroscopy in the range 1–40 eV. We found optical band gap thresholds of 1.9, 1.4, and 1.1 eV for the mono-, bi-, and trilayer BP, respectively. The experimental data are simulated to determine the quasiparticle gap (E_g), the optical gap (E_x), and the corresponding exciton binding energy (E_b) for various effective dielectric constants, which provide an abacus of the optical response of BP as a function of dielectric environment. The variation of the electronic gap in few-layer BP is found to be sizably larger than the variation of the binding energy. In bulk BP, experimental and calculated plasmon dispersions along the two orthogonal directions display a significant anisotropy both in amplitude and in shape. A progressive linearization of the dispersion of the volume and surface plasmons is observed in both experimental and theoretical data of monolayer and bilayer BP. These results highlight the importance of strong quantum confinement effects in the optical properties of thin-layer BP and pave the way for tuning them by tailoring the dielectric environment.

Methods. The black phosphorus crystals used in this work were purchased from HQ Graphene. BP was stored and exfoliated in a glovebox with regenerated Ar system to maintain the oxygen and moisture concentrations below 1 ppm. Exfoliation of BP and the transfer of the flake on a TEM grid were performed using PDMS stamps (Sylgard 184) cured at 70 °C for 25 min (details in the Supporting Information). We used 300 mesh holey carbon on a copper grid with mark to localize the flakes. The TEM grid is then placed on a tilt-

rotation sample holder inside the glovebox. The sample holder is finally sealed in a custom transfer plastic bag with a 40 mbar pressure of Ar and transferred to the TEM chamber for experiments.

■ ASSOCIATED CONTENT

S Supporting Information

The Supporting Information is available free of charge on the ACS Publications website at DOI: 10.1021/acs.nanolett.9b03928.

Sample fabrication, HAADF images, layer number determination, and computational details (PDF)

■ AUTHOR INFORMATION

Corresponding Authors

*E-mail: etienne.gaufres@u-bordeaux.fr.

*E-mail: annick.loiseau@onera.fr.

ORCID

Etienne Gaufrès: 0000-0002-5122-1423

Lorenzo Sponza: 0000-0003-4094-5570

Zhenglu Li: 0000-0002-3851-9241

Steven G. Louie: 0000-0003-0622-0170

Richard Martel: 0000-0002-9021-4656

Michel Côté: 0000-0001-9046-9491

Annick Loiseau: 0000-0002-1042-5876

Author Contributions

E.G. and F.F. performed the experiments; E.G., F.F., A.L., and R.M. designed the experiments and analyzed the results; E.G. prepared the samples; V.G., L.S., F.D., M.C., Z.L., and S.G.L. performed the simulations; E.G. and A.L. supervised the work. All authors contributed to the scientific discussions, manuscript preparation, and final version.

Notes

The authors declare no competing financial interest.

■ ACKNOWLEDGMENTS

This work received funding from the European Union's Horizon 2020 research and innovation program under Grant Agreement Nos. 696656 (Graphene Core 1) and 785219 (Graphene Core 2) and from the ANR french program under Grant Agreement No. ANR-17-CE24-0023-01 (EPOS-BP). E.G. acknowledges funding from the Marie-Sklodowska-Curie-IF 706476-BrightPhoton, the GDR-I Graphene and Co, and the GDR-I multifunctional nanomaterials for travel support. V.G. and M.C. would like to acknowledge the support of the Fonds de Recherche du Québec - Nature et Technologie (FRQNT), the Natural Sciences and Engineering Research Council of Canada (NSERC), under grant RGPIN-2016-06666. R.M. acknowledges support from Canada Research Chair and NSERC under grants RGPIN-2019-06545 and RGPAS-2019-00050. Part of the simulations were performed on computers provided by the Canadian Foundation for Innovation, the Ministère de l'Éducation des Loisirs et du Sport (Québec), Calcul Québec, and Compute Canada. Z.L. and S.G.L. acknowledge support from the van der Waals Heterostructures program (KCWF16) at the Lawrence Berkeley National Lab through the Office of Science, Office of Basic Energy Sciences, Materials Sciences and Engineering Division, the U.S. Department of Energy, under Contract No. DE-AC02-05CH11231, which provided for the calculations of dielectric responses using the BerkeleyGW package. The

advanced computational methods and codes were provided by the Center for Computational Study of Excited-State Phenomena in Energy Materials (C2SEPEM) funded by the U.S. Department of Energy, Office of Basic Energy Sciences, Materials Sciences and Engineering Division, under Contract No. DE-AC02-05CH11231 at the Lawrence Berkeley National Laboratory, as part of the Computational Materials Sciences Program.

■ REFERENCES

- (1) Li, L.; Yu, Y.; Ye, G. J.; Ge, Q.; Ou, X.; Wu, H.; Feng, D.; Chen, X. H.; Zhang, Y. Black phosphorus field effect transistors. *Nat. Nanotechnol.* **2014**, *9*, 372–377.
- (2) Qiao, J.; Kong, X.; Hu, Z.-X.; Yang, F.; Ji, W. High-mobility transport anisotropy and linear dichroism in few layer black phosphorus. *Nat. Commun.* **2014**, *5*, 4475.
- (3) Liu, H.; Neal, A. T.; Zhu, Z.; Luo, Z.; Xu, X.; Tomanek, D.; Ye, P. D. Phosphorene, An unexpected 2D semiconductor with a high hole Mobility. *ACS Nano* **2014**, *8* (4), 4033–4041.
- (4) Tayari, V.; Hemsworth, N.; Kakih, I.; Favron, A.; Gaufrès, E.; Gervais, G.; Martel, R.; Szkopek, T. Two-dimensional magnetotransport in a black phosphorus naked quantum well. *Nat. Commun.* **2015**, *6*, 7702.
- (5) Long, G.; Maryenko, D.; Shen, J.; Xu, S.; Hou, J.; Wu, Z.; Wong, W. K.; Han, T.; Lin, J.; Cai, Y.; Lortz, R.; Wang, N. Achieving ultrahigh carrier mobility in two-dimensional hole gas of black phosphorus. *Nano Lett.* **2016**, *16* (12), 7768–7773.
- (6) Favron, A.; Gaufrès, E.; Fossard, F.; Phaneuf-L'Heureux, A.-L.; Tang, Y.-W.; Levesque, P.; Loiseau, A.; Leonelli, R.; Francoeur, S.; Martel, R. Photo-oxidation and quantum confinement effects in exfoliated black phosphorus. *Nat. Mater.* **2015**, *14*, 826–832.
- (7) Li, L.; Kim, J.; Jin, C.; Ye, G. J.; Qiu, D. Y.; da Jornada, F. H.; Shi, Z.; Chen, L.; Zhang, Z.; Yang, F.; Watanabe, K.; Taniguchi, T.; Ren, W.; Louie, S. G.; Chen, X. H.; Zhang, Y.; Wang, F. Direct observation of the layer-dependent electronic structure in phosphorene. *Nat. Nanotechnol.* **2017**, *12*, 21–25.
- (8) Wang, X.; Jones, A. M.; Seyler, K. L.; Tran, V.; Jia, Y.; Zhao, H.; Wang, H.; Yang, L.; Xia, F. Highly anisotropic and robust excitons in monolayer black phosphorus. *Nat. Nanotechnol.* **2015**, *10* (6), 517–521.
- (9) Thomson, D.; Zilkie, A.; Bowers, J. E.; Komljenovic, T.; Reed, G. T.; Vivien, L.; Marris-Morini, D.; Cassan, E.; Virot, L.; Fédeli, J.-M.; Hartmann, J.-M.; Schmid, J. H.; Xu, D.-X.; Boeuf, F.; O'Brien, P.; Mashanovich, G. Z.; Nedeljkovic, M. Roadmap on silicon photonics. *J. Opt.* **2016**, *18*, 073003.
- (10) Raja, A.; Chaves, A.; Yu, J.; Arefe, G.; Hill, H. M.; Albert, F.; Rigosi, A. F.; Berkelbach, T. C.; Nagler, P.; Schüller, C.; Korn, T.; Nuckolls, C.; Hone, J.; Brus, L. E.; Heinz, T. F.; Reichman, D. R.; Chernikov, A. Coulomb engineering of the bandgap and excitons in two-dimensional materials. *Nat. Commun.* **2017**, *8*, 15251.
- (11) Gerber, I. C.; Marie, X. Dependence of band structure and exciton properties of encapsulated WSe₂ monolayers on the hBN-layer thickness. *Phys. Rev. B: Condens. Matter Mater. Phys.* **2018**, *98*, 245126.
- (12) Walsh, A. G.; Vamivakas, A. N.; Yin, Y.; Cronin, S. B.; Ünlü, M. S.; Goldberg, B. B.; Swan, A. Screening of excitons in single, suspended carbon nanotubes. *Nano Lett.* **2007**, *7* (6), 1485–1488.
- (13) Aspitarte, L.; McCulley, D. R.; Bertoni, A.; Island, J. O.; Ostermann, M.; Rontani, M.; Steele, G. A.; Minot, E. D. Giant modulation of the electronic band gap of carbon nanotubes by dielectric screening. *Sci. Rep.* **2017**, *7*, 8828.
- (14) Scheuschner, N.; Ochedowski, O.; Kaulitz, A.-M.; Gillen, R.; Schleberger, M.; Maultzsch, J. Photoluminescence of freestanding single- and few-layer MoS₂. *Phys. Rev. B: Condens. Matter Mater. Phys.* **2014**, *89*, 125406.
- (15) Lin, Y.; Ling, X.; Yu, L.; Huang, S.; Hsu, A. L.; Lee, Y.-H.; Kong, J.; Dresselhaus, M. S.; Palacios, T. Dielectric screening of excitons and trions in single layer MoS₂. *Nano Lett.* **2014**, *14* (10), 5569–5576.
- (16) Stier, A. V.; Wilson, N. P.; Clark, G.; Xu, X.; Crooker, S. A. Probing the influence of dielectric environment on excitons in monolayer WSe₂: Insight from high magnetic fields. *Nano Lett.* **2016**, *16* (11), 7054–7060.
- (17) Deng, Y.; Luo, Z.; Conrad, N. J.; Liu, H.; Gong, Y.; Najmaei, S.; Ajayan, P. M.; Lou, J.; Xu, X.; Ye, P. D. Black phosphorus - monolayer MoS₂ van der Waals Heterojunction p-n diode. *ACS Nano* **2014**, *8* (8), 8292–8299.
- (18) Qiu, D. Y.; da Jornada, F. H.; Louie, S. G. Environmental screening effect in 2D materials, Renormalization of the band gap, electronic structure and optical spectra of few layer black phosphorus. *Nano Lett.* **2017**, *17* (8), 4706–4712.
- (19) Brockt, G.; Lakner, H. Nanoscale EELS analysis of dielectric function and bandgap properties in GaN and related materials. *Micron* **2000**, *31*, 435–440.
- (20) Erni, R.; Browning, N. D. Quantification of the size-dependent energy gap of individual CdSe quantum dots by valence electron energy-loss spectroscopy. *Ultramicroscopy* **2007**, *107*, 267–273.
- (21) Virdi, K. S.; Kauffmann, Y.; Ziegler, C.; Ganter, P.; Blaha, P.; Lotsch, B. V.; Kaplan, W. D.; Scheu, C. Band gap extraction from individual two dimensional perovskite nanosheets using valence electron energy loss spectroscopy. *J. Phys. Chem. C* **2016**, *120*, 11170–11179.
- (22) Park, J.; Heo, S.; Chung, J. – G.; Kim, H.; Lee, H.; Kim, K.; Park, G. – S. Bandgap measurement of thin dielectric films using monochromated STEM-EELS. *Ultramicroscopy* **2009**, *109* (9), 1183–1188.
- (23) Tizei, L. H. G.; Lin, Y. – C.; Mukai, M.; Sawada, H.; Lu, A. – Y.; Li, L. – J.; Kimono, K.; Suenaga, K. Exciton mapping at subwavelength scales in two-dimensional materials. *Phys. Rev. Lett.* **2015**, *114*, 107601.
- (24) Dileep, K.; Sahu, R.; Sarkar, S.; Peter, S. C.; Dalta, R. Layer specific optical band gap measurement at nanoscale in MoS₂ and ReS₂ van der Waals compounds by high resolution electron energy loss spectroscopy. *J. Appl. Phys.* **2016**, *119*, 114309.
- (25) Williams, D. B.; Carter, C. B. *Transmission Electron Microscopy, a Textbook for Materials Science*; Springer Science + Business Media: New York, 2009; Part 3: Imaging, Chapter 22, pp 379–388.
- (26) Frank, T.; Derian, R.; Tokár, K.; Mitas, L.; Fabian, J.; Štich, I. Many-body quantum Monte Carlo study of 2D materials: Cohesion and bandgap in single-layer phosphorene. *Phys. Rev. X* **2019**, *9*, 011018.
- (27) Prada, E.; Alvarez, J. V.; Narasimha-Acharya, K. L.; Bailen, F. J.; Palacios, J. J. Effective-mass theory for the anisotropic exciton in two-dimensional crystals: Application to phosphorene. *Phys. Rev. B: Condens. Matter Mater. Phys.* **2015**, *91*, 245421.
- (28) Yang, J.; Xu, R.; Pei, J.; Myint, Y. W.; Wang, F.; Wang, Z.; Yu, Z.; Lu, Y. Unambiguous identification of monolayer phosphorene by phase-shifting interferometry. 2014, arXiv:1412.6701. arXiv.org e-Print archive. <https://arxiv.org/abs/1412.6701>.
- (29) Kern, L.-M.; Galceran, R.; Zatko, V.; Galbiati, M.; Godel, F.; Perconte, D.; Bouamrane, F.; Gaufrès, E.; Loiseau, A.; Brus, P.; Bezencenet, O.; Martin, M.-B.; Servet, B.; Petroff, F.; Dlbak, B.; Seneor, P. Atomic layer deposition of a MgO barrier for passivated black phosphorus spintronics platform. *Appl. Phys. Lett.* **2019**, *114* (5), 053107.
- (30) Wirtz, L.; Marini, A.; Rubio, A. Excitons in boron nitride nanotubes: Dimensionality effects. *Phys. Rev. Lett.* **2006**, *96*, 126104.
- (31) Fossard, F.; Sponza, L.; Schué, L.; Attaccalite, C.; Ducastelle, F.; Barjon, J.; Loiseau, A. Angle-resolved electron energy loss spectroscopy in hexagonal boron nitride. *Phys. Rev. B: Condens. Matter Mater. Phys.* **2017**, *96*, 115304.
- (32) Hong, J.; Li, K.; Jin, C.; Zhang, X.; Zhang, Z.; Yuan, J. Layer-dependent anisotropic electronic structure of freestanding quasi-two-dimensional MoS₂. *Phys. Rev. B: Condens. Matter Mater. Phys.* **2016**, *93*, 075440.

- (33) Wachsmuth, P.; Hambach, R.; Kinyanjui, M. K.; Guzzo, M.; Benner, G.; Kaiser, U. High-energy collective electronic excitations in free-standing single-layer graphene. *Phys. Rev. B: Condens. Matter Mater. Phys.* **2013**, *88*, 075433.
- (34) Wu, R. J.; Topsakal, M.; Low, T.; Robbins, M. C.; Haratipour, N.; Jeong, J. S.; Wentzcovitch, R. M.; Koester, S. J.; Mkoyan, K. A. Atomic and electronic structure of exfoliated black phosphorus. *J. Vac. Sci. Technol., A* **2015**, *33*, 060604.
- (35) Nicotra, G.; van Veen, E.; Deretzis, I.; Wang, L.; Hu, J.; Mao, Z.; Fabio, V.; Spinella, C.; Chiarello, G.; Rudenko, A.; Yuan, S.; Politano, A. Anisotropic ultraviolet-plasmon dispersion in black phosphorus. *Nanoscale* **2018**, *10*, 21918–21927.
- (36) Gonze, X.; Jollet, F.; Abreu Araujo, F.; Adams, D.; Amadon, B.; Appelcourt, T.; Audouze, C.; Beuken, J.-M.; Bieder, J.; Bokhanchuk, A.; Bousquet, E.; Bruneval, F.; Caliste, D.; Cote, M.; Dahm, F.; Da Pievè, F.; Delaveau, M.; Di Gennaro, M.; Dorado, B.; Espejo, C.; Geneste, G.; Genovese, L.; Gerossier, A.; Giantomassi, M.; Gillet, Y.; Hamann, D.R.; He, L.; Jomard, G.; Laflamme Janssen, J.; Le Roux, S.; Levitt, A.; Lherbier, A.; Liu, F.; Lukacevic, I.; Martin, A.; Martins, C.; Oliveira, M.J.T.; Ponce, S.; Pouillon, Y.; Rangel, T.; Rignanese, G.-M.; Romero, A.H.; Rousseau, B.; Rubel, O.; Shukri, A.A.; Stankovski, M.; Torrent, M.; Van Setten, M.J.; Van Troeye, B.; Verstraete, M.J.; Waroquier, D.; Wiktor, J.; Xu, B.; Zhou, A.; Zwanziger, J.W. Recent Developments in the ABINIT Software Package. *Comput. Phys. Commun.* **2016**, *205*, 106–310.
- (37) Deslippe, J.; Samsonidze, G.; Strubbe, D. A.; Jain, M.; Cohen, M. L.; Louie, S. G.; Berkeley, G. W. A Massively Parallel Computer Package for the Calculation of the Quasiparticle and Optical Properties of Materials and Nanostructures. *Comput. Phys. Commun.* **2012**, *183*, 1269.
- (38) Ghosh, B.; Kumar, P.; Thakur, A.; Chauhan, Y. S.; Bhowmick, S.; Agarwal, A. Anisotropic plasmons, excitons and electron energy loss spectroscopy of phosphorene. *Phys. Rev. B: Condens. Matter Mater. Phys.* **2017**, *96*, 035422.
- (39) Low, T.; Roldà, R.; Wang, H.; Xia, F.; Avouris, P.; Moreno, L. M.; Guinea, F. Plasmons and screening in monolayer and multilayer black phosphorus. *Phys. Rev. Lett.* **2014**, *113*, 106802.
- (40) Kramberger, C.; Hambach, R.; Giorgetti, C.; Rümmeli, M. H.; Knupfer, M.; Fink, J.; Bücher, B.; Reining, L.; Einarsson, E.; Maruyama, S.; Sottile, F.; Hannewald, K.; Olevano, V.; Marinopoulos, A. G.; Pichler, T. Linear plasmon dispersion in single wall carbon nanotubes and the collective excitation spectrum of graphene. *Phys. Rev. Lett.* **2008**, *100*, 196803.